World Conference on Timber Engineering Oslo 2023

FINITE ELEMENT ANALYSIS OF BUCKLING BEHAVIOR OF TIMBER ENCASED STEEL COMPOSITE COLUMNS SUBJECTED TO AXIAL LOAD

Ying Gao[1], Feiyang Xu[2], Minghao Geng[3], Qibin Hu[4], Xinmiao Meng[5]

ABSTRACT: Timber encased steel composite (TESC) columns provide a feasible application to large-scale and high-rise structures. This paper investigates the axial load distribution and buckling behavior of TESC columns with embedded H-section steel through finite element (FE) analysis combined with parametric studies. The numerical results revealed that increasing the slenderness ratio could enhance the confinement effect of the timber in improving the maximum load. A larger proportion of timber area provided a more significant confinement effect in enhancing the ductility of the steel, and then a minimum area ratio for TESC columns considering the confinement effect of timber was determined.

KEYWORDS: Finite element analysis, Steel-timber composite column, Load distribution, Parametric study

1 INTRODUCTION

The use of wood for construction purposes has increasingly been the subject of investigations in past decades due to its significant sustainability superiorities such as carbon sequestration and low environmental impact [1]. Timber-steel composite structures have been demonstrated as effective structural solutions for modern timber structures. Benefiting from the composite systems with reasonable design, the disadvantages of wood can be minimized to some extent, while the advantages of steel and timber can be fully utilized.

Timber encased steel composite (TESC) column is a steel-timber composite member with remarkable potential for multi-story timber buildings that have been increasingly needed in recent years. Typically, the steel is fully embedded in the glulam and connected through adhesives, [2]. The use of steel, on the one hand, can effectively improve the stiffness and strength of the column without increasing or not significantly increasing the column size, which is beneficial to structural design such as indoor space utilization. On the other hand, it alleviates the issue of the shortage of wood resources in China and is conducive to the promotion and application of timber in construction. Meanwhile, the outer timber not only provides lateral confinement on the inner steel to enhance the strength but also offers anti-corrosion and fire-retardant coating for the inner steel. The TESC column has been applied as fire-resistant structural columns in timber structures such as the Wood Square Building [3]. TESC columns could be prefabricated in the factory, ensuring product quality and on-site assembly efficiency. Although the cost of the TESC column will increase compared with the glulam column, it is expected that the improvement of the structural performance of TESC columns can offset this increase.

Several experimental studies have been conducted to investigate the mechanical behavior of TESC columns with different configurations. [2, 4-7] Significant improvements in the stiffness and load-carrying capacity of TESC columns were observed. However, the application of TESC columns is inhibited to some extent due to the lack of design methods. A choice should be made between the steel and the timber design methods or made based on both methods. The root of the choice lies in an insightful evaluation concerning the load distribution of each component in the composite column and the interaction at the interface, which is critical for structural design. In this regard, more efforts are needed to gain insight into the structural responses and establish relevant design methods. Nonetheless, the load distribution and interaction are difficult to monitor during the tests. Thus, performing numerical studies to fill the gaps is an available and significant approach to structural analysis [8].

In this paper, a numerical investigation on the axial load distribution and buckling behavior of TESC columns with embedded H-section steel is described. The proposed FE models are built via ABAQUS and validated through experimental results from previous studies [2]. Parametric studies are then performed to evaluate the effects of variations in geometric parameters and material strengths on the compressive behavior of the encased steel column by analyzing the axial load distribution on steel and timber of TESC columns.

[1] Ying Gao, BFU Beijing Forestry University, China, gaoying@bjfu.edu.cn
[2] Feiyang Xu, BFU Beijing Forestry University, China, xufeiyang1996@bjfu.edu.cn
[3] Minghao Geng, BFU Beijing Forestry University, China, gmh7210406@bjfu.edu.cn
[4] Qibin Hu, UA University of Alberta, Canada, qibin@ualberta.ca
[5] Xinmiao Meng, BFU Beijing Forestry University, China, mengxinmiao@bjfu.edu.cn

https://doi.org/10.52202/069179-0417

2 AXIAL COMPRESSION TESTS OF TYPICAL TESC COLUMNS

Axial compression tests of TESC columns were performed by Hu et al. [2]. The glulam of the column was made of first-grade Douglas-fir. The moisture content of the tested samples was approximately 12%. The mean density was 480 kg/m^3. The inner steel was wide flange hot-rolled H-section steel (Q235B class) with sectional dimensions of 125 × 125 × 6.5 × 9 mm. The resorcinol adhesive was used to produce the glulam and the two-component epoxy adhesive was applied to connect the glulam and steel. The width (D) of the square TESC column was 226 mm. The manufacturing process of the TESC column is shown in Figure 1(a). A total of 6 TESC specimens were tested with lengths of 1100 mm, 1700 mm and 2300 mm. The loading protocol was according to standard GB/T 50329–2012 [9], and the test setup is displayed in Figure 1(b). The axial compression tests were conducted with the same moisture content. The support conditions of the specimen were fixed at the bottom and hinged at the top. Strength failure of 1100 mm long specimens and global buckling of 1700 and 2300 mm specimens was observed. as shown in Figures. 1(c). The load–axial displacement curves are shown in Figure 1(d) The load-axial strain behavior, initial stiffness, load-carrying capacity and ductility were determined (see Hu et al. [2]). The previous test results provide a basis for the calibration of the FE models.

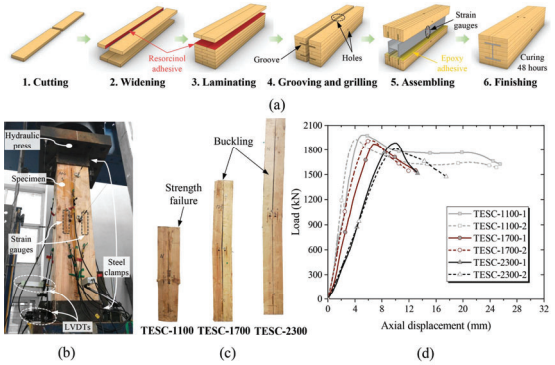

Figure 1: *Summary of axial compression tests: (a) fabrication of the TESC column, (b) test setup, (c) typical failure modes and (d) load-axial displacement curves [2]*

3 FINITE ELEMENT ANALYSIS

3.1 MATERIALS

The elasto-plastic constitutive law was adopted for timber [10]. The elastic behavior of timber was defined as orthotropic through the Engineering Constants in ABAQUS, and the properties are listed in Table 1. The compressive MOE E_L and strength f_{ct} parallel to the grain of timber were determined by axial compression tests on two short full-scale glulam columns. The plastic behavior was characterized by the Hill yield criterion for anisotropic materials [11].

Table 1: *Material properties of timber*

Property		Timber	CoV (%)
Elastic Modulus (MPa)	E_L	13600	3.12
	E_R [7]	577.9	16.70
	E_T [7]	424.2	9.01
Poisson's Ratio [13]	u_{LR}	0.292	
	u_{LT}	0.449	
	u_{RT}	0.390	
Shear Modulus (MPa) [13]	G_{LR}	870.4	
	G_{LT}	1060.8	
	G_{RT}	95.2	
Compressive strength (MPa)	Parallel	26.32	7.45

Note: L, R and T represent the axial, radial and tangential directions of timber, respectively.

The material properties of the steel were obtained through tensile tests. The average MOE E_s and yield strength f_y were taken as 206 GPa and 280 MPa, respectively. The elastic-plastic isotropic behavior was considered and a multilinear stress-strain relationship was adopted in FE models. The Poisson's ratio was set to 0.3.

3.2 MODELING

The FE models were built using the software ABAQUS. The 8-node linear brick element with reduced integration (C3D8R) was selected to simulate the steel and timber. For simplicity, the following steps were adopted: the arc at the flange-web junction of the H-section steel was taken as the right angle due to the negligible effect on the simulation results. However, the six pre-drilled holes (diameter = 20 mm) for threading through the strain gauges in actual TESC columns were considered, given that it significantly affected the failure modes of the specimens [7]; each glulam was regarded as an entirety without glue delamination [14]; the tie constraint was set to simulate the contact between steel and timber due to a near full composite action before reaching the maximum load observed in the tests [2, 5, 7].

The boundary conditions and meshing are shown in Figure 2. A reference point coupled with the top surface of the column was established for applying the load and boundary conditions. The top and bottom surface of the specimen was constrained as a hinge end and a fixed end, respectively.

A mesh convergence test was carried out by element refinement. The global size of the characteristic element varied from 20, 15 and 10 mm. Considering the computational accuracy and efficiency, the global size of the characteristic element was set as 15 mm. The FE models were loaded using a displacement-control procedure in a quasi-static state. The displacement was directly applied to the reference point at the top surface.

The first buckling mode obtained from the eigenvalue buckling prediction was adopted as the initial geometric imperfection distribution, and its magnitude was taken as 1/1000 of the column length.

https://doi.org/10.52202/069179-0417

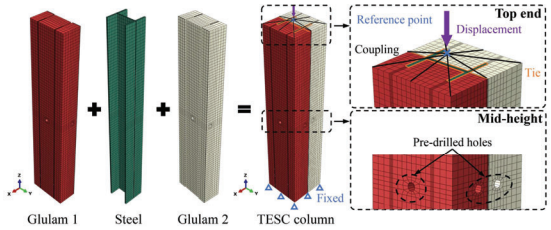

Figure 2: *Geometric modeling of the TESC column*

3.3 SIMULATION VALIDATION

The numerical results were compared and discussed with the experimental results. The numerical failure modes exhibited good agreement with the test observations, as shown in Figure 3. The local damage caused by the pre-drilled holes at the mid-height of the column was well simulated by FE models. It should be noted that the pre-drilled holes increase the influence of the geometry of the TESC column on its buckling performance, thus weakening the ability of FE models to verify the correctness of the material properties of timber to a certain extent. Nevertheless, the built FE models remain reliable since the pre-drilled holes affect the buckling capacity of the TESC column to the same extent. If the strength of the timber is too large or too small, it will lead to significant errors. In addition, the FE model could not predict the cracking at the post-peak stage since the adhesive layers were neglected. The numerical load-axial displacement curves displayed a relatively good trend with test results, as displayed in Figures 4(a) to (c). Nevertheless, the initial slope of numerical curves in the elastic stage was slightly higher, which was commonly observed [15, 16]. The initial differences between FE models and physical specimens, as well as the relatively large deformation at the specimen end, may cause the higher axial displacement recorded from the LVDTs, thus exhibiting a lower initial stiffness in the experimental curves. The load-axial strain relationships of timber were further used to validate the FE modeling methods, especially the elastic behavior, as shown in Figures 8(b) to (f). It was found that the numerical results showed excellent consistency with the experimental results.

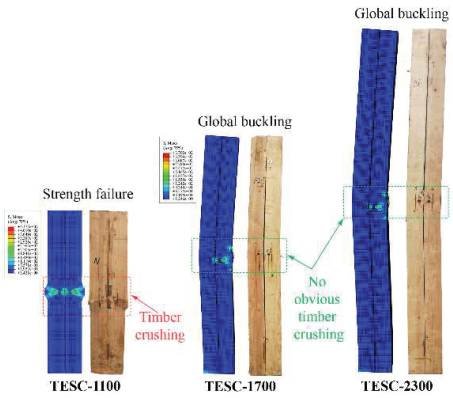

Figure 3: *Comparison of deformation and damage of TESC specimens observed in experiments and FE models.*

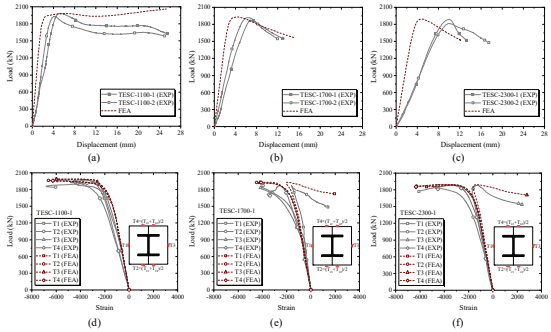

Figure 4: *Comparison between numerical and experimental results: (a), (b) and (c) load-axial displacement curves; (d), (e) and (f) load-axial strain curves of timber*

The authors also performed a finite element analysis on the axial compressive behavior of 16 L-shaped TESC columns with the same materials in this paper but a different cross-sectional shape [7]. The differences between numerical results and experimental results are basically within 10% and the reliability of FE models was validated. Although the section of the simulated TESC column is different, the same modeling methods were adopted. Therefore, it can be further proved that The proposed modeling approaches show to be sufficiently accurate in predicting the axial compressive behavior of the TESC columns.

3.4 LOAD DISTRIBUTION

The validated FE models were used to analyze the load distribution on individual components of the TESC column. The load on each component was extracted through the function of “Free body cut” in ABAQUS. Figure 5 shows the load-axial displacement curves of TESC columns and components. ‘IS’ and ‘OT’ respectively represent the inner steel and outer timber in the TESC column, and ‘TESC’ represents the composite column. The yield point was determined by the farthest-pointing method [17].

The failure sequence of steel and timber was shown from the analysis of load distribution on components. The steel yielding occurred earlier than the timber and TESC column, with a load level of approximately 40% of the load-carrying capacity. It results from the relatively small steel ratio (5.77%) of the TESC column, even though the steel yield strength is much larger than the timber compressive strength. The specimen TESC-1100 entered the yield stage almost synchronously with the timber. In contrast, the yield displacement of specimen TESC-2300 was closer to that of the steel. It implies that with an increasing slenderness ratio, the crucial component that determines the yield of the TESC column changes from timber to steel. It is worth noting that both the timber and steel components almost simultaneously reached their maximum load with the TESC column, indicating a

https://doi.org/10.52202/069179-0417

perfect composite effect with the full utilization of different materials being achieved. The residual load-carrying capacity of steel in the specimen TESC-1100 was kept stable due to the sufficient lateral restraint provided by the timber. However, the load allocated on components in specimens TESC-1700 and TESC-2300 gradually decreased after reaching the maximum load due to the global buckling.

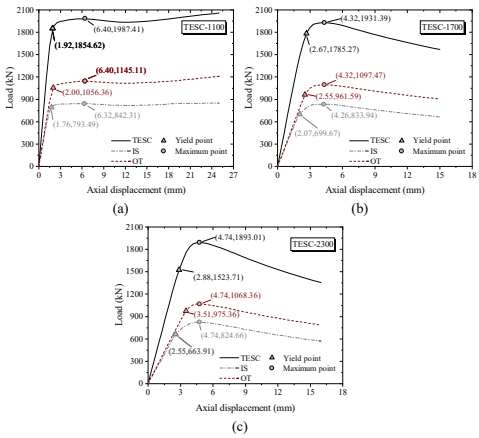

Figure 5: *Load distribution on components of specimens: (a) TESC-1100, (b) TESC-1700 and (c) TESC-2300*

To assess the confinement effect provided by the timber on steel, the load-axial displacement curves of each component in the TESC column and the bare parts were compared, as shown in Figure 6. “S” and “T” represent the bare steel column and bare timber column, respectively. Take specimens with a length of 2300 mm as an example. It was found that the confinement effect provided by the timber on steel was primarily reflected in enhancing the load-carrying capacity and ductility. The confinement effect was activated after the yielding of the steel component, allowing the steel component in the TESC column to exhibit a smoother yielding stage and a higher maximum load than the bare steel column. The bare steel column reached the maximum load of approximately 713 kN at 3.20 mm, while the steel component reached the maximum load of approximately 825 kN at 4.80 mm. Furthermore, the outer timber suppressed the post-buckling behavior of the inner steel, thus leading to a substantially higher residual load-carrying capacity than that of the bare steel column. However, the load-carrying capacity of the timber component was lower than the bare timber column. The bare timber column reached the maximum load of approximately 1195 kN at 5.80 mm, while the timber component of the TESC column reached the maximum load of approximately 1068 kN at 4.80 mm. It is because the timber component is in the field of axial compression and lateral pressure, which weakened the load-carrying capacity of the timber.

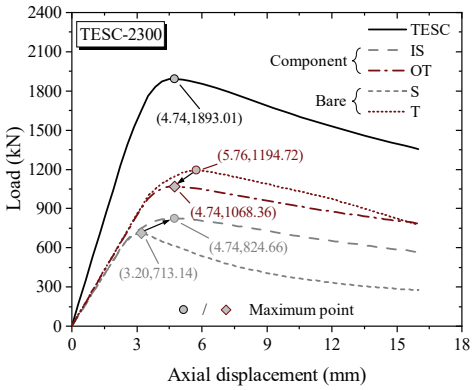

Figure 6: *Comparison of load on components and individual loaded parts*

4 PARAMETRIC STUDY

Based on the validated FE modeling, a parametric study was conducted to evaluate the influence of geometric and material parameters on the compressive behavior of TESC columns and the load distribution on components. The parameters were categorized into two groups. The first group A focused on the strength-related parameters, including the steel yield strength and the compressive strength parallel to the grain of timber. The second group B regarding the geometric-related variables, including the steel area, timber area and slenderness ratio.

The details of the parameters are listed in Table 2. The steel yield strengths changed from 235, 345, 460, and 960 MPa. According to [13], three commonly used wood species of Engelmann Spruce (*Picea engelmannii*), Red Pine (*Pinus resinosa*) and Western Larch (*Larix occidentalis*) were selected. The average compressive strengths parallel to the grain are 30.9 MPa, 41.9 MPa and 52.5 MPa, respectively. Five types of H-section steel with different steel areas were chosen from the standard GB/T 11263—2017 [18]. The steel ratio (A_s/A_{TESC}) by the steel sectional area A_s and the TESC column sectional area A_{TESC} was used to describe the specimen with the same composite area but different steel areas. The area ratio (A_{TESC}/A_s) was used to describe the specimen with different timber areas but the same steel area. The value of A_{TESC}/A_s was determined by the cross-section width D (ranging from 125 mm to 260 mm) of the TESC column or the width t (ranging from 0 mm to 50 mm) of the encased timber between the H-section steel shown in Figure 10(b). The slenderness ratio λ changed from approximately 5 to 200. The corresponding column lengths L were taken as 500, 1100, 1700, 2300, 2900, …, and 16300 mm. The increment of the length was 600 mm. The λ was calculated as follows.

$$\lambda = \frac{KL}{i} \tag{1}$$

https://doi.org/10.52202/069179-0417

$$i = \sqrt{\frac{I_t + I_s E_s / E_t}{A_t + A_s f_y / f_{ct}}} \quad (2)$$

where K represents the effective length factor. Since the top end of the TESC column was hinged and the bottom end was fixed, the value of K was set to 0.7. The radius of gyration of the cross-section i was calculated by Eq. (2) according to [19], where I_s and I_t were the moments of inertia of the steel and timber components around the minor-axis of H-section steel, respectively. The column TESC-2300 was selected as the control specimen of the parametric study considering that the column length of 2300 mm was common in practical applications. A total of 140 FE models, including the corresponding bare steel columns and timber columns, were built and analyzed. It should be noted that the predrilled holes at the mid-height specially designed for the strain measurement of the inner steel in tests, were not considered in the parametric study.

Table 2. *Investigated parameters in the parametric study*

Group	Steel yield strength f_y (GPa)	Timber strength f_{ct} (MPa)	Steel ratio (Steel sectional dimensions, $b \times d \times t_w \times t_f$, mm)	Width t/D (mm)	Area ratio A_{TESC}/A_s	Length L (mm)
A	235 345 460 690 960	26.32	5.77% (125 × 125 × 6.5 × 9)	226	17.34	2300
	280	26.32 30.9 41.9 52.5	4.12% (100 × 100 × 6 × 8)	226	24.28	2300
		26.3 30.9 41.9 52.5	5.77% (125 × 125 × 6.5 × 9)		17.34	
		26.3 30.9 41.9 52.5	7.66% (150 × 150 × 7 × 10)		13.06	
B	280	26.32	4.12% (100 × 100 × 6 × 8) 5.77% (125 × 125 × 6.5 × 9) 7.66% (150 × 150 × 7 × 10) 9.78% (175 × 175 × 7.5 × 11) 12.15% (200 × 200 × 8 × 12)	226	24.28 17.34 13.06 10.22 8.23	2300
	280	26.32	5.77% (125 × 125 × 6.5 × 9)	0 40 125 140 160 185 226 260	1.00 3.91 5.30 6.65 8.69 11.62 17.34 22.95	2300
	280	26.32	4.12% (100 × 100 × 6 × 8)	226	24.28	500, 1100, 1700, …, 16500
			5.77% (125 × 125 × 6.5 × 9)		17.34	500, 1100, 1700, …, 16500
			7.66% (150 × 150 × 7 × 10)		13.06	500, 1100, 1700,

https://doi.org/10.52202/069179-0417

Note: The steel ratio was calculated as $A_s/A_{TESC} \times 100\%$; When the value of t/D is less than 125, it represents t, otherwise it represents D.

To evaluate the confinement effect provided by the timber on steel, the maximum load enhancement N_{ens} and the ductility enhancement μ_{ens} of the steel component were defined and calculated as follows.

$$N_{ens} = \frac{N_{IS}}{N_S} \tag{3}$$

$$\mu_{ens} = \frac{\mu_{IS}}{\mu_S} \tag{4}$$

where N_{IS} and μ_{IS} represent the maximum load and ductility of the steel component, respectively. N_S and μ_S denote the maximum load and ductility of the bare steel column under axial loading, respectively. The ductility μ was calculated as follows.

$$\mu = \frac{d_u}{d_y} \tag{5}$$

where d_y and d_u are the displacements corresponding to the yield load and ultimate load, respectively. The ultimate load of the steel was the load when the load dropped to 85% of the maximum load.

4.1 STEEL YIELD STRENGTH

The load-axial displacement curves of TESC columns and their components with different steel yield strengths are shown in Figure 7. It was assumed that the constitutive relationship of the steel was less influenced by the strength grade, so the consistent stress-strain relationship was adopted for the steel. The trends of curves shown in Figure 7(a) indicate that although steel contributed a small percentage of the total sectional area, increasing the steel yield strength could remarkably enhance the maximum load of the composite column. A significant strength enhancement of 73.07% is achieved when the steel yield strength increased from 235 MPa to 960 MPa. Moreover, it could be seen from Figures 7(b) and (c) that the load-carrying capacity of the composite column was mainly provided by the steel component when the steel yield strength was larger than 460 MPa. An interesting finding was observed in Figure 7(c) that increasing the steel yield strength led to a higher maximum load of the timber. It can be explained by the fact that the yield of the TESC column is delayed when the steel yield strength increases, thus can fully utilize the compressive strength of the timber. Nonetheless, the TESC column with a higher steel yield strength exhibited a slightly less ductile response, even though the higher residual load-carrying capacity at the end of the analysis was observed.

The enhancement of maximum load and ductility of the steel component is shown in Figure 7(d). When the steel yield strength increased from 235 MPa to 960 MPa, the value of N_{ens} and μ_{ens} decreased in general, indicating that the confinement effect is insufficient for the higher grade steel. In other words, reducing the strength differences between timber and steel can receive a better confinement effect for the steel. Furthermore, the value of μ_{ens} was much higher than that of N_{ens}, showing that the confinement effect provided by timber influences the ductility of the inner steel more than the strength.

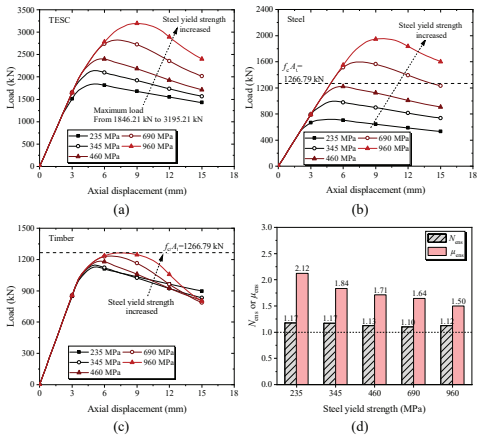

Figure 7: *Comparison of load-axial displacement relationships with different steel yield strengths: (a) TESC column, (b) steel component, (c) timber component and (d) enhancement of maximum load and ductility*

4.2 STEEL AREA

The load-axial displacement curves of TESC columns with different steel ratios are shown in Figure 8. As expected, the larger steel ratio contributed to the higher stiffness and load-carrying capacity of the TESC column, as shown in Figure 8(a). When the steel ratio increased from 4.12% to 12.15%, the initial stiffness and maximum load were enhanced by 72.01% and 56.23%, respectively. It can be seen in Figure 8(b) that such enhancement results from the contribution of the steel component. Meanwhile, Figure 8(c) shows that the stiffness and maximum load of the timber component decreased when the steel ratio increased due to the relative decrease in the timber area.

The comparison of maximum load enhancement and ductility enhancement of the steel component and the individual part is shown in Figure 8(d). With the increase of the steel ratio from 4.12% to 12.15%, the values of N_{ens} and μ_{ens} decreased, indicating that the higher steel ratio leads to the lower confinement effect provided by timber, and the steel ratio should be less than 12.15% in the proposed TESC columns. Furthermore, it can also be seen that the ductility showed higher sensitivity to the steel ratio than the maximum load.

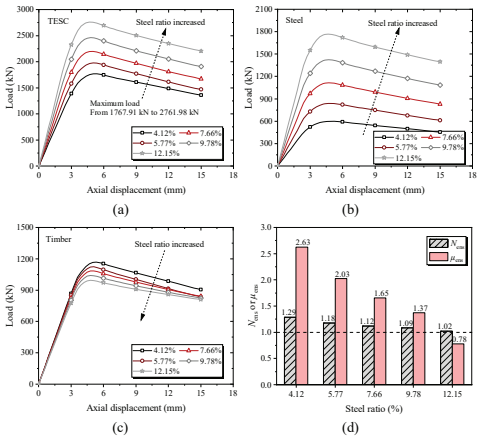

Figure 8: *Comparison of load-axial displacement relationships with different steel ratios: (a) TESC column, (b) steel component, (c) timber component and (d) enhancement of maximum load and ductility of steel*

4.3 TIMBER STRENGTH

The maximum load of TESC columns with different compressive strengths parallel to the grain of timber and steel ratios are compared in Figure 9(a). Similar to the effects of the steel yield strength, the higher value of f_{ct} also led to the higher maximum load of TESC columns. Using a higher grade of timber is an effective method to enhance the capacity of the composite column due to the much larger sectional area proportion of the timber component. For the TESC column with a larger steel ratio, however, a lower enhancement of the load-carrying capacity of the TESC column was observed. It indicates that the TESC column with high timber compressive strength and a large steel ratio may not be economic in terms of load-carrying capacity. It was also found that the effect of increasing timber compressive strength on improving the steel component capacity was not significant. Take specimens with a steel ratio of 5.77 % as an example. The load-axial displacement curves of the steel component are shown in Figure 9(b). Only less than 6% of the enhancement of maximum load was gained. It may result from the steel already reaching its yield strength. In this regard, increasing the compressive strength of timber allows the steel to experience a more pronounced yield plateau accompanied by a larger maximum displacement. In conclusion, it is reasonable to consider that the response of improving timber compressive strength on the steel component is mainly reflected in the hardening effect after the yielding of the steel.

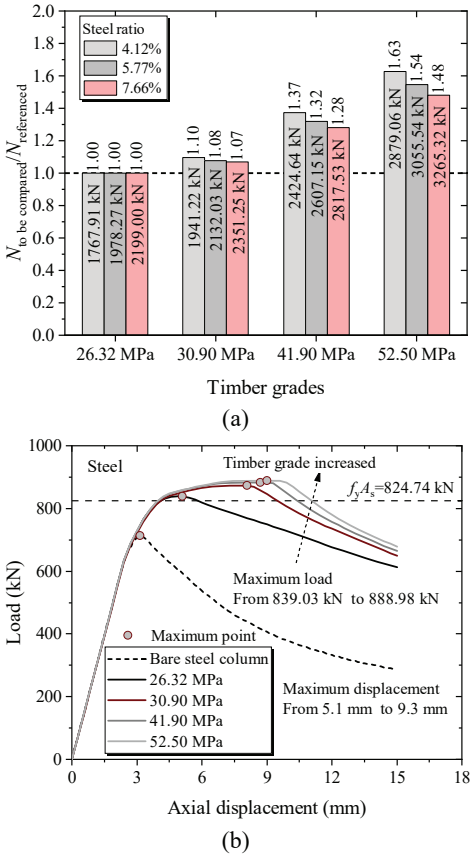

Figure 9: *The influence of timber compressive strength: (a) enhancement of maximum load of TESC columns and (b) load-axial displacement curves of the steel component in TESC columns with the steel ratio of 5.77%*

4.4 AREA RATIOS A_{TESC}/A_S

The effects of timber area on the steel component are discussed and analyzed in this section, as shown in Figure 10. It should be noted that when $A_{TESC}/A_S < 5.30$, the steel component is partially covered by timber, while the steel is fully coated by timber when $A_{TESC}/A_S > 5.30$.

Figure 10(a) shows that the influence of an increasing timber area followed a similar trend to the decrease of the steel ratio, with the enhanced maximum load and the ductile response of the steel. In the case of $A_{TESC}/A_S < 5.30$, increasing timber area slightly improved the load-carrying capacity and ductility of the steel component, as shown in Figure 10(b). It is because the buckling of the steel flanges is not well restrained since the steel is not fully covered. For $A_{TESC}/A_S > 5.30$, the mechanical performance of the steel component, especially ductility, was significantly improved. More than twice times enhancement of ductility was obtained when A_{TESC}/A_S was increased to approximately 23, whereas the value of the strength was only enhanced by approximately 20%. It is noteworthy that the steel could reach the yield strength when the value of A_{TESC}/A_S was 11.62. A slight enhancement of strength was observed when $A_{TESC}/A_S > 11.62$. The results revealed

https://doi.org/10.52202/069179-0417

that before reaching the steel yield strength, increasing the timber area greatly improves both the load-carrying capacity and the ductility of the steel component. After that, the effects of such an increase are mainly reflected in suppressing the post-buckling behavior of the steel component.

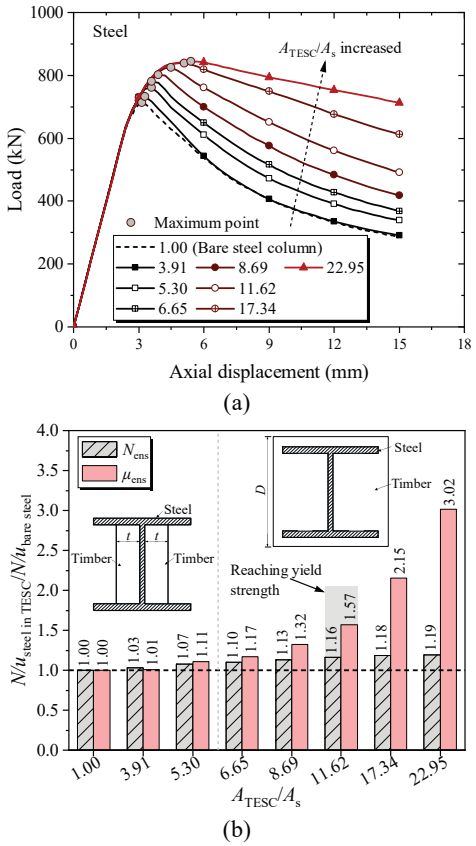

Figure 10: *Comparison of the steel component and the bare steel column: (a) load-axial displacement curves and (b) enhancement of maximum load and ductility*

The results mentioned above imply that the strength of the steel component might not be fully utilized with a relatively thin timber coating. Consequently, there is a minimum ratio of A_{TESC}/A_S (ξ_{min}) to ensure the steel component could reach the strength capacity under axial compression [20]. A parametric study was conducted to identify the value of ξ_{min}. The length-to-width ratio (L/d) of the steel component was defined, where d was the flange width of the H-section steel and was set to 125 mm (sectional dimensions of the steel: 125 × 125 × 6.5 × 9 mm) in this case. The column length L changed from 1000 mm to 3500 mm. Three steel yield strengths, namely 235, 280 and 345 MPa, were adopted. The relationship between ξ_{min} and L/d is shown in Figure 11(a). It was found that as L/d increased, a larger ξ_{min} was needed to provide enough lateral confinement. Subsequently, linear relationships are proposed to calculate the ξ_{min} as follows.

$$\xi_{min} = k\left(L/d - r_0\right) + s_0 \quad (6)$$

where k is the slope of the design curve, r_0 is the smallest L/d to ensure that the bare steel column could reach the yield strength under axial compression, and s_0 is the minimum ξ_{min} related to the sectional area of the steel component, which is taken as 5.30 in this work. The recommended values of parameters in Eq. (6) are shown in Figure 11(b). The ratios of calculation to simulation results were within the range of 0.85 to 1, indicating that the proposed design curves are safe. Meanwhile, it avoids material waste due to overly conservative calculation results.

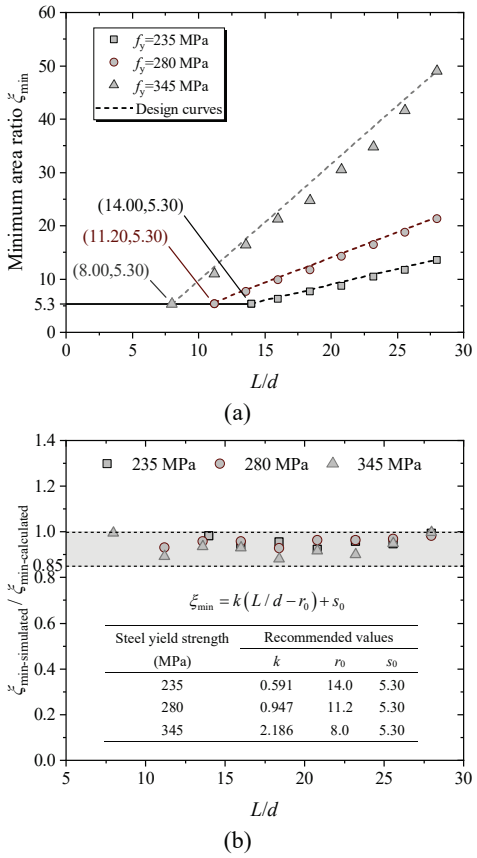

Figure 11: *Calculation results: (a) design curves and (b) comparison between calculation and numerical results*

4.5 SLENDERNESS RATIO

The influences of the slenderness ratio on the load-carrying capacity of the steel component were investigated. The TESC columns with steel ratios of 4.12%, 5.77% and 7.66% were selected in this section. The sectional dimensions of TESC columns were 226 ×

226 mm. The non-dimensional slenderness λ_n was used and calculated as follows.

$$\lambda_n = \sqrt{\frac{N_p}{N_{cr}}} = \frac{KL}{\pi}\sqrt{\frac{f_y A_s + f_{ct} A_t}{E_s I_s + E_t I_t}} = \frac{\lambda}{\pi}\sqrt{\frac{f_{ct}}{E_t}} \quad (7)$$

$$N_p = f_y A_s + f_{ct} A_t \quad (8)$$

$$N_{cr} = \frac{\pi^2 (E_s I_s + E_t I_t)}{(KL)^2} \quad (9)$$

Considering that the steel was converted into timber in Eq. (2), only the parameters of timber (f_{ct}/E_t) were adopted in Eq. (7). Relationships between the enhancement of the maximum load of the steel component and the non-dimensional slenderness are shown in Figure 12(a). The maximum load was nonlinearly enhanced with an increasing slenderness ratio. Three distinctive stages are observed. In stage A ($\lambda_n < \lambda_b$), the TESC column exhibited strength failure and the maximum load increased slowly. In stage B ($\lambda_b < \lambda_n < \lambda_{cr}$), the elasto-plastic instability dominated the failure mode of the composite column. A substantial amount of the load-carrying capacity recovered owing to the lateral restraint of timber, thus remarkably improving the maximum load when the slenderness ratio increased. In stage C ($\lambda_{cr} < \lambda_n$), the increase rate of the maximum load enhancement slowed down and tended to be stable since the elastic instability governed the failure mode. In addition, the smaller steel ratio of the TESC column contributed to the higher load enhancement of the steel component.

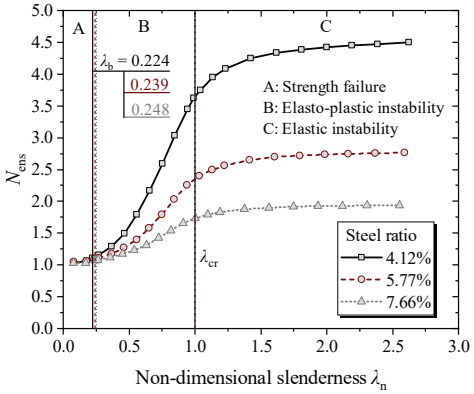

(a)

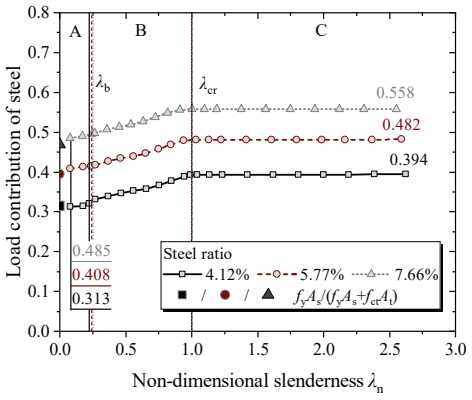

(b)

Figure 12: *Influence of slenderness ratios on the steel component: (a) enhancement of maximum load and (b) load contribution of steel*

The load contribution of the steel component when the TESC column reached the maximum load was compared, as shown in Figure 12(b). It was observed that the larger steel ratio led to the higher load contribution of the steel component. Owing to the confinement effect, the minimum load contribution ratio of the steel in the investigated slenderness ratios is slightly higher than the value of $f_yA_s/(f_yA_s+f_{ct}A_t)$. When it entered stage B, the elasto-plastic instability occurred and the curves almost linearly increased. After that, the load contribution of the steel component kept stable with a negligible improvement. It is due to the occurrence of elastic instability, the much high second-order effect results in the load-carrying capacity of the slender TESC column being independent of the material strength. In conclusion, the steel component carries an increasing percentage of the maximum load of the TESC column when the slenderness ratio increases.

5 CONCLUSIONS

The axial load distribution and buckling behavior of TESC columns with embedded H-section steel were investigated via a thorough numerical investigation in this work. The proposed FE modeling approaches of TESC columns reasonably simulated the experimental responses. The numerical results showed that the steel influenced the yield of the TESC column more than timber under a large slenderness ratio. Additionally, the increase in column length also led to a large load enhancement of the steel component compared with the bare steel column.

Parametric studies revealed that the geometry parameters exhibited more influence than the material strength on the compressive behavior of TESC columns and the encased steel. For a TESC column with a certain slenderness ratio, the maximum load of steel increased significantly with a larger area ratio when the minimum area ratio was not reached. While the ductility of the steel increased remarkably with a larger area ratio when the minimum area ratio was reached. For a TESC column with a certain

https://doi.org/10.52202/069179-0417

area ratio, either reducing the steel yield strength or enhancing the timber compressive strength could benefit the compressive performance of the steel. In addition, increasing the slenderness ratio led to a larger load contribution of the steel when the TESC column reached the maximum load.

The minimum area ratio of the TESC column was determined considering the inner steel could reach the yield strength. A thicker timber coating was required with an increase in either yield strength or length-to-width ratio of the inner steel. The proposed design curves regarding the area ratio and length-to-width ratio of the steel could be used for determining the scale of the TESC column.

ACKNOWLEDGEMENT

The authors gratefully acknowledge the National Natural Science Foundation of China under Grant [number 51908038] and the National Key R&D Program of China under Grant [number 2021YFB2301602] for supporting this research.

REFERENCES

[1] Churkina G, Organschi A, Reyer CPO, Ruff A, Vinke K, Liu Z et al. Buildings as a global carbon sink. *Nature Sustainability*, 3:269-76, 2020.

[2] Hu Q, Gao Y, Meng X, Diao Y. Axial compression of steel–timber composite column consisting of H-shaped steel and glulam. *Engineering Structures*, 216:110561, 2022.

[3] Quintana GP, Carradine DM, Bazaez R. State of the art and practice of seismic-resistant hybrid timber structures. *European Journal of Wood and Wood Products*,79:5-28, 2020.

[4] Mikio K, Hiroshi I, Shuitsu Y. The design and installation of a five-story new timber building in Japan. *Proceedings of the Summaries of Technical Papers of Annual Meeting Japan Society for Finishing Technology*, Tokio, Japan, 2005.

[5] Kia L, Valipour H.R. Composite timber-steel encased columns subjected to concentric loading. *Engineering Structures*, 232:111825, 2021.

[6] Kusumoto S, Shioya S, Kawabe R, Inomoto K. Innovative Hybrid Timber Structure in Japan Beam-To-Beam Moment Resisting Connection. *World Conference on Timber Engineering. Vienna*, Austria, 2016.

[7] Xu F, Xuan S, Li W, Meng X, Gao Y. Compressive performance of steel-timber composite L-shaped columns under concentric loading. *Journal of Building Engineering*, 48:103967, 2022.

[8] Tao Z, Wang Z, Yu Q. Finite element modelling of concrete-filled steel stub columns under axial compression. *Journal of Constructional Steel Research*. 89:121-31, 2013.

[9] GB/T 50329-2012. Standard for test methods of timber structures. Ministry of Housing and Urban-Rural Development of the People's Republic of China, Beijing, China Architecture Publishing Press, 2012.

[10] Li Z, He M, Wang X, Li M. Seismic performance assessment of steel frame infilled with prefabricated wood shear walls. *Journal of Constructional Steel Research*, 140:62-73, 2018.

[11] Hill R. The mathematical theory of plasticity. London: Oxford University Press, 1950.

[12] Navaratnam S, Thamboo J, Pologanathan K, Roy K, Gatheeshgar P. Finite element modelling of timber infilled steel tubular short columns under axial compression. *Structure*, 30:910-24, 2021.

[13] Ross RJ. Wood handbook—Wood as an engineering material. Madison, WI: U.S.: General Technical Report FPL-GTR-190, Department of Agriculture, Forest Products Laboratory; 2010.

[14] Ehrhart T, Steiger R, Palma P, Gehri E, Frangi A. Glulam columns made of European beech timber: compressive strength and stiffness parallel to the grain, buckling resistance and adaptation of the effective-length method according to Eurocode 5. *Materials and Structures*, 53:1-12, 2020.

[15] Liang H, Li W, Huang Y, Lu Y. Axial behavior of CFST stub columns strengthened with steel tube and sandwiched concrete jackets. *Thin-Walled Structures*, 155:106942, 2020.

[16] Aslani F, Uy B, Tao Z, Mashiri F. Behavior and design of composite columns incorporating compact high-strength steel plates. *Journal of Constructional Steel Research*, 107:94-110, 2015.

[17] Feng P, Cheng S, Bai Y, Ye L. Mechanical behavior of concrete-filled square steel tube with FRP-confined concrete core subjected to axial compression. *Composite Structures*, 123:312-24, 2015.

[18] GB/T 11263—2017. Hot rolled H and cut T section steel. Beijing, China Standardization Administration, 2017.

[19] CECS 159:2004 Technical specification for structures with concrete-filled rectangular steel tube members. Beijing, China Association for Engineering Construction Standardization, 2004.

[20] Wang Z, Feng P, Zhao Y, Yu T. FRP-confined concrete core-encased rebar for RC columns: Concept and axial compressive behavior. *Composite Structures*, 222:110915, 2019.